ADVANCED MATERIALS
www.advmat.de

# In Situ Interweaved High Sulfur Loading Li–S Cathode by Catalytically Active Metalloporphyrin Based Organic Polymer Binders

*Xiaoman Yao, Can Guo, Chunlei Song, Meng Lu, Yuluan Zhang, Jie Zhou, Hui-Min Ding, Yifa Chen,* Shun-Li Li, and Ya-Qian Lan**

**The elaborate design of powerful Li–S binders with extended-functions like polysulfides adsorption/catalysis and $Li^+$ hopping/transferring in addition to robust adhesion-property has remained a challenge. Here, an in situ cathode-interweaving strategy based on metalloporphyrin based covalent-bonding organic polymer (M-COP, M = Mn, Ni, and Zn) binders is reported for the first time. Thus-produced functional binders possess excellent mechanical-strengths, polysulfides adsorption/catalysis, and $Li^+$ hopping/transferring ability. Specifically, the modulus of Mn-COP can reach up to ≈54.60 GPa (≈40 times higher than poly(vinylidene fluoride)) and the relative cell delivers a high initial-capacity (1027 mAh $g^{-1}$, 1 C and 913 mAh $g^{-1}$, 2 C), and excellent cycling-stability for >1000 cycles even at 4 C. The utilization-rate of sulfur can reach up to 81.8% and the electrodes based on these powerful binders can be easily scale-up fabricated (≈20 cm in a batch-experiment). Noteworthy, Mn-COP based cell delivers excellent capacities at a high sulfur-loading (8.6 mg $cm^{-2}$) and low E/S ratio (5.8 μL $mg^{-1}$). In addition, theoretical calculations reveal the vital roles of metalloporphyrin and thiourea-groups in enhancing the battery-performance.**

## 1. Introduction

Li–S battery has become the most promising energy storage system due to its overwhelming theoretical specific energy (2567 Wh $kg^{-1}$) and capacity (1675 mAh $g^{-1}$).[1–3] Nevertheless, Li–S battery still have some shortcomings, such as the notorious lithium polysulfides (LiPSs) shuttle problem, destruction of electrode structural integrity by volume expansion, and dendrite growth of Li anode, leading to the poor cycling stability and undesired battery performance.[1,4] Nowadays, some researchers have proposed the "four high" ("4H") and "four low" ("4L") criteria to evaluate the applicability of Li–S battery, in which 4H refers to the capacity value > 1200 mAh $g^{-1}$, $m_{sl}$ > 8 mg $cm^{-2}$, $R_{Cathode}$ > 70 wt%, Coulombic efficiency >99.9% and 4L indicates porosity < 60%, $R_{N/P}$ < 3, $R_{E/S}$ < 3 μL $mg^{-1}$ and the minimal inactive material.[5] However, these criteria seem to be hardly met at the current research stages. To approach these high criteria, every fundamental component in Li–S battery needs to be designed comprehensively and systematically.[6] As a kind of minor and important component in electrode, binders (mostly occupy <10 wt% in cathode), presenting adhesion and structural/mechanical stabilization ability, could play a decisive role in the performance improvement of Li–S battery to some extent yet is generally neglected.[6–8] Currently, polymer binders have been commonly investigated and can be classified into four main categories (i.e., fluoro-polymers, conductive polymers, ionic polymers, and water-soluble polymers),[9] among which poly(vinylidene fluoride) (PVDF) has been the most studied one due to its potential in commercial applications. However, the adhesion of PVDF lies in the relatively weak inter-chain van der Waals forces, leading to the swelling effect in electrolytes and poor binder performance during battery tests.[10,11] To substitute PVDF and extend the intrinsic scope of binders, a desirable Li–S battery binder would better present advanced properties like LiPSs adsorption/catalysis or $Li^+$ hopping/transferring in addition to the basic adhesion. Therefore, the design of novel and multifunctional polymer binders to meet the high criteria would be highly demanded to replace PVDF for the next-generation Li–S battery.

Up to date, a series of polymer binders containing polar functional groups have been developed as pioneering substitutes to replace PVDF, such as modified fluoro-polymer binders P(VDF-TRFE),[12] cross-linked carboxymethylcellulose citric acid (CMC-CA),[13] polyamide amine (PAMAM) dendrimer,[14,15]

X. Yao, C. Guo, C. Song, M. Lu, Y. Zhang, J. Zhou, Y. Chen, S.-L. Li, Y.-Q. Lan
National and Local Joint Engineering Research Center of MPTES in High Energy and Safety LIBs
Engineering Research Center of MTEES (Ministry of Education)
Key Laboratory of ETESPG(GHEI)
School of Chemistry
South China Normal University
Guangzhou 510006, P. R. China
E-mail: chyf927821@163.com; yqlan@njnu.edu.cn
H.-M. Ding
School of Chemistry and Materials Science
Nanjing Normal University
Nanjing 210023, P. R. China

The ORCID identification number(s) for the author(s) of this article can be found under https://doi.org/10.1002/adma.202208846.

**DOI: 10.1002/adma.202208846**

or water-soluble functional polymer binder (GN-BA), etc.[11] Despite the promising properties that have been achieved, they still have bottlenecks like: 1) most of the reported polymer binders are focused on the properties of LiPSs adsorption, other vital functions such as LiPSs catalytic conversion or $Li^+$ hopping/transferring have been rarely explored;[16,17] 2) most of the works have applied synthesized polymer binders as adhesive agents through ex situ fabrication processes, which would be short in the interaction with cathodic materials (i.e., carbon nanotube (CNT) and S), and 3) there are rare polymer binders with reported battery performances that can partially meet high requirements of "4H" or "4L." Notably, the ex situ fabrication processes would increase the tendency of imprecise electrode fabrication/manufacturing failure, resulting in the binder accumulation at the surface,[18] active particles exfoliation/self-agglomeration, or more drastic volume expansion to trigger the rapid attenuation of capacity.[19,20] Aiming at these challenges, reasonable cathode fabrication strategies including 3D-printing electrode technology,[21] capillary deposition method,[22] electrospinning technology,[23] atomic layer deposition,[24] or mechanical mixing[25] have been studied, yet this field is still at the early stage and there are some unresolved issues need to be carefully addressed. In this context, the exploration of both novel polymer binders and in situ cathode fabrication techniques might be feasible and essential for high-performance Li–S battery.

Herein, an in situ cathode interweaving strategy has been explored via a series of metalloporphyrin based covalent-bonding organic polymer (M-COP, M = Mn, Ni, and Zn) binders, during which the in situ heating polymerization of binders can simultaneously provide strong interaction with cathodic materials and accomplish one-pot cathode fabrication (**Figure 1**). Interestingly, the obtained M-COP (M = Mn, Ni, and Zn) binders assembled from metalloporphyrin and thiourea groups show high mechanical strength/adhesion, strong LiPSs adsorption/catalysis, and $Li^+$ hopping/transferring ability, which can tightly interweave cathodic materials (i.e., CNT and S) as a compact whole and be facilely fabricated in large scale (≈20 cm in a batch experiment). Best of them, Mn-COP/CNT/S based cell delivers an initial specific capacity of 1027 mAh $g^{-1}$ at 1 C, 913 mAh $g^{-1}$ at 2 C, and excellent cycling stability for >1000 cycles (0.064% decay per cycle) at 4 C. Moreover, the cell exhibits a high specific capacity of 1029.9 mAh $g^{-1}$ at a low E/S ratio of 8.1 µL $mg^{-1}$, and an excellent capacity of 949.2 mAh $g^{-1}$ even when the E/S ratio is reduced to 5.8 µL $mg^{-1}$. Noteworthy, Mn-COP/CNT/S based cell also enables the high sulfur loading of 8.6 mg $cm^{-2}$, in which the achieved initial area capacity and specific capacity can be as high as 7.8 mA h $cm^{-2}$ and 909.8 mA h $g^{-1}$ at 0.1 C, respectively. Besides, the functions of metalloporphyrin and thiourea groups like LiPSs adsorption/catalysis and $Li^+$ hopping/transferring have been intensively studied by the density functional theory (DFT) calculations and sufficient characterizations. These definite explorations of such powerful metalloporphyrin based binders and novel cathode fabrication techniques would pave the way to realize high-performance electrochemical energy devices for portable power electronics.

## 2. Results and Discussion

### 2.1. Synthesis and Characterization

M-COP (M = Mn, Ni, and Zn) were prepared through a facile heating polymerization process with the assembly of metalloporphyrin (MTAPP, M = Mn, Ni, and Zn) and 1,4-diisocyanate (PDI) via a thiourea-forming condensation reaction (for details see Experimental Section) (**Figure 2**a). To verify the composition of samples, Fourier-transform infrared spectroscopy (FTIR) tests were conducted to detect the characteristic groups of M-COP (M = Mn, Ni, and Zn). Taking Mn-COP as an example, the obvious characteristic stretching

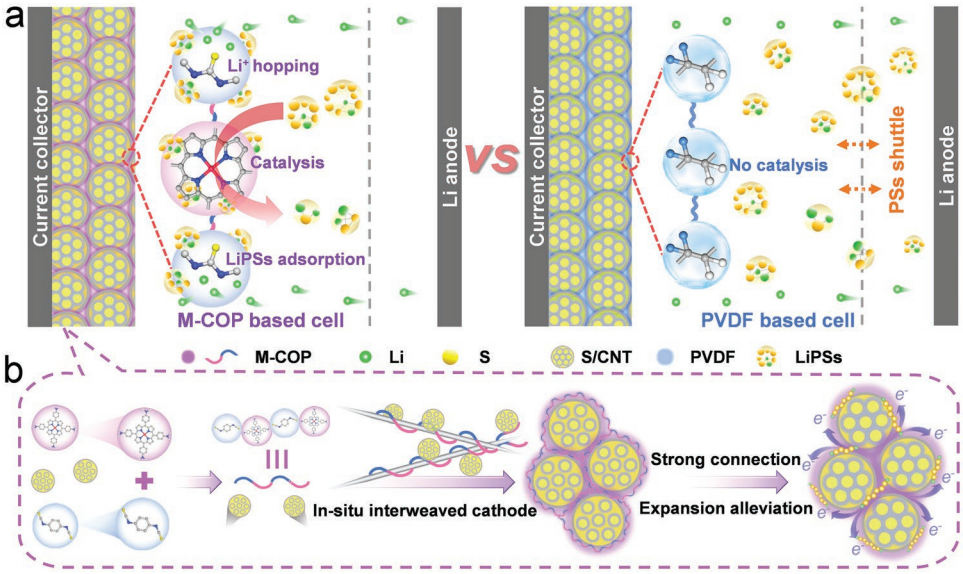


**Figure 1.** The schematic illustration of the in situ cathode interweaving strategy based on the covalent-bonding organic polymer (M-COP, M = Mn, Ni, and Zn) binders. a) The advantages of M-COP based cell versus PVDF based cell. b) The schematic illustration of in situ cathode interweaving strategy.

 

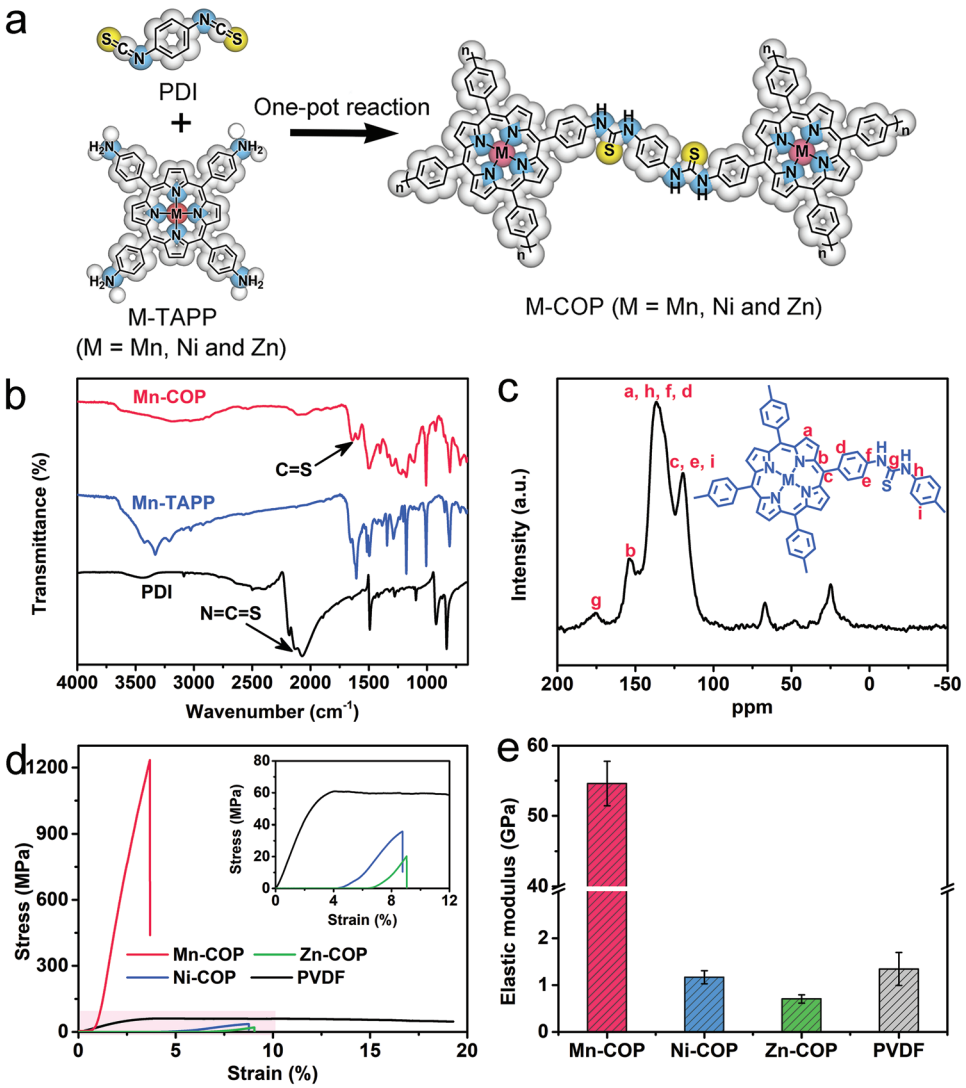


**Figure 2.** Structure and characterization of M-COP (M = Mn, Ni, and Zn). a) The syntheses and structures of M-COP (M = Mn, Ni, and Zn). b) FTIR spectra of PDI, Mn-TAPP, and Mn-COP. c) $^{13}C$ NMR spectrum of M-COP. d) Stress–strain curves of different binders. e) Elastic modulus of different binders.

band (2000–2200 $cm^{-1}$) of the isothiocyanate group in PDI disappears, while two peaks of N—C=S (1500 $cm^{-1}$) and N—H (3350 $cm^{-1}$) ascribing to thiourea group emerge obviously, suggesting the formation of thiourea bond in Mn-COP (Figure 2b). Besides, the C=N stretching vibration band (1620 $cm^{-1}$) belonging to Mn-TAPP maintains almost unchanged in Mn-COP,[26] implying that the retained Mn-porphyrin unit in Mn-COP. Similarly, the successful formation of Ni-COP and Zn-COP is also confirmed by their relative FTIR tests (Figure S1, Supporting Information). In addition, the solid-state $^{13}C$ NMR spectrum displays a characteristic peak (i.e., 175 ppm) of C=S for thiourea group.[27] Furthermore, the detected peaks are analyzed and can be assigned to the relative carbon atoms in porphyrin unit (i.e., a, b, and c) and phenyl (i.e., d, e, f, h, and i) (Figure 2c), respectively, further supporting the above FTIR results.[28,29] As expected, the powder X-ray diffraction (PXRD) results exhibit the amorphous characteristics of these polymer materials (Figure S2, Supporting Information). Moreover, the elements and chemical bonds of polymer materials were characterized and analyzed by X-ray photoelectron spectroscopy (XPS) tests. In the XPS spectra of M-COP (M = Mn, Ni, and Zn), three main peaks with the binding energy of ≈284.6, ≈411.1, and ≈699.1 eV belong to C 1s, N 1s, and S 2p, respectively (Figure S3, Supporting Information).[30] For instance, four peaks of Mn-COP at 284.6 eV, 285.2 eV, 286.0 eV, and 287.6 eV in C 1s spectrum represent the C=C, C—N, C=N, and C=S groups, respectively (Figure S4, Supporting Information). Besides, the satellite peak at 400.1 eV is ascribed to the porphyrin unit, while the peaks at 398.3 eV and 399.1 eV are consistent with that of pyrrolic N and amine groups in N 1s spectrum, respectively.[31,32] Furthermore, the Mn 2p spectrum of Mn-COP displays two deconvolution peaks located at 653.8 eV and 642.5 eV, which indicates the bivalent state of Mn (Figure S4, Supporting Information).[33] In addition, the bivalent states of Zn and Ni

for Zn-COP and Ni-COP have also been proved by their relative XPS spectra (Figures S5 and S6, Supporting Information).[34]

Scanning electron microscope (SEM) and energy-dispersive X-ray spectroscopy (EDS) element mapping tests were carried out to characterize the relative morphology of M-COP (M = Mn, Ni, and Zn) in the film forms. Taking Mn-COP for instance, it shows a smooth surface and Mn, S, and N are evenly distributed in Mn-COP (Figure S7, Supporting Information). Similar results have also been detected for Ni-COP and Zn-COP (Figures S8,S9, Supporting Information). The uniformly distributed morphology with strong covalent bonding might impart them with high mechanical strength. Thus, the strain–stress curves have been plotted to visualize the mechanical behaviors of these binders in the film forms. It should be mentioned that Mn-COP can withstand the maximum tensile stress of (1.23 GPa, 3.67%), which is much superior to Ni-COP (0.036 GPa, 8.76%) and Zn-COP (0.020 GPa, 9.04%) (Figure 2d). In sharp contrast, the tensile stress property of Mn-COP is ≈20 times higher than that of PVDF, suggesting the strong covalent-bond and $\pi$–$\pi$ interaction might join together to largely enhance the mechanical property. Moreover, the modulus of Mn-COP can be as high as 54.60 GPa, which is ≈40, ≈47, and ≈78 times higher than those of PVDF, Ni-COP, and Zn-COP (Figure 2e). The incredible modulus might make the cathode materials more tightly connected when they are applied as functional binders, which is very conducive to resisting the stress caused by the volume expansion of the cathode.

If the binder is stretched or sheared when mixed with solid particles, the dynamic characteristic is very important for the stabilization of the binder and solid particles.[35] Thus, the shear rheological experiments were carried out and the result showed that Mn-COP exhibited significantly higher viscosity than PVDF (**Figure 3**a; Figure S10, Supporting Information).

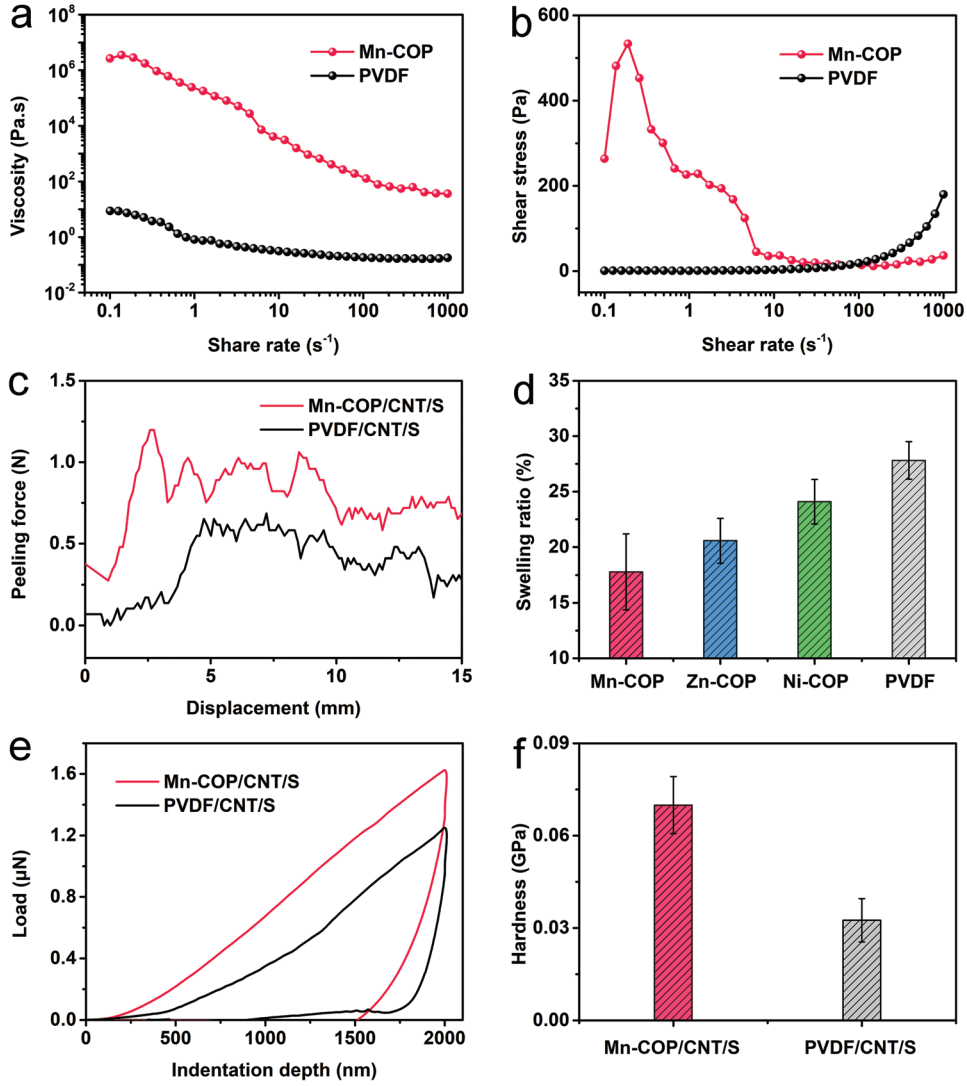


**Figure 3.** Characterizations of different binders. a) Viscosity as a function of shear rate for Mn-COP and PVDF. b) Shearing adhesion strength of Mn-COP and PVDF. c) Peel-off strength profiles of Mn-COP/CNT/S and PVDF/CNT/S electrodes. d) Swelling ratios of M-COP/CNT/S (M = Mn, Ni, and Zn) and PVDF/CNT/S electrodes. e) Nanoindentation profiles of Mn-COP/CNT/S and PVDF/CNT/S electrodes. f) The hardness of Mn-COP/CNT/S and PVDF/CNT/S electrodes.

Furthermore, the mechanical strength of Mn-COP and PVDF was tested by estimating their shearing adhesion. As shown in the shear stress-rate curves, the shear strength of Mn-COP is much higher than that of PVDF (Figure 3b). The strong shearing strength of Mn-COP can effectively provide a strong binding ability to enable the fabrication of a robust cathode and would be much beneficial for the cathode to better endure the volume expansion during the electrochemical charge and discharge processes.[32,33]

Based on the above-mentioned properties, we further set out to explore their potential as binders in Li–S cathode. In detail, we reported an in situ cathode interweaving strategy based on the synthesis processes of M-COP (M = Mn, Ni, and Zn) binders, during which the in situ heat polymerization process of binders can simultaneously provide strong interaction with cathodic materials (CNT and S) and accomplish one-pot cathode fabrication (for details, see Experimental Section). After casting the mixed slurry of CNT, S, and binder precursors (i.e., M-TAPP and PDI) onto the current collector and heating, an integrated cathode was produced by the one-pot method for further characterizations. In order to certify the advantages of M-COP (M = Mn, Ni, and Zn) when applied to the cathode, the physical properties of them have been evaluated. The 180° peeling tests with a stretching velocity of 10 mm $min^{-1}$ were used to evaluate the adhesion properties of Mn-COP and PVDF, and the results demonstrated that the Mn-COP/CNT/S electrode required more force than PVDF/CNT/S under the same displacement (Figure 3c). This reveals that Mn-COP with the superior adhesion to PVDF can more effectively inhibit the peeling and falling of the active materials. To test their anti-swelling effect, the electrodes based on different binders have been submerged in the electrolyte solution for 24 h and the mass difference of the electrode before and after soaking has been weighed. The results display that the electrodes with Mn-COP (≈17.8%), Ni-COP (≈20.6%), and Zn-COP (≈24.1%) as the binders all have lower weight increments while the electrode with PVDF (≈27.8%) swells easily in electrolyte (Figure 3d). The appropriate swelling rate of these M-COP/CNT/S (M = Mn, Ni, and Zn) electrodes would be more favorable to simultaneously maintain the good wettability of the electrolyte and avoid the excessive absorption of electrolyte.[36] In addition, the robust mechanical strength and excellent adhesion of them were further characterized by the nano-indentation measurement. Taking Mn-COP/CNT/S electrode as an example, the force imposed on the electrode is higher than that of the PVDF/CNT/S electrode when the indentation depths are the same at 2000 nm (Figure 3e).[37,38] Moreover, the hardness and modulus at different positions were also measured at the maximum indentation depth of the probe (Figure 3f; Figure S11, Supporting Information). As a result, the higher Young's modulus and hardness of the Mn-COP/CNT/S electrode than PVDF/CNT/S electrode imply that it would possess higher mechanical performance and binding strength to restrain the volume expansion of the cathodes.[39] In addition to these properties, the strong adhesion is further reflected in the photograph images of the folding test, proving the superiority of Mn-COP to PVDF (Figure S12, Supporting Information) and it can be facilely fabricated in a large scale (≈20 cm in a batch experiment) (Figure S13, Supporting Information).

To evaluate the adsorption and catalytic conversion of LiPSs by M-COP (M = Mn, Ni, and Zn) binders, the LiPSs adsorption experiments were carried out. An equal amount of Mn-COP, Ni-COP, Zn-COP, and PVDF polymers were immersed into the same volume of $Li_2S_6$ solution. After 24 h, the solutions with Mn-COP, Ni-COP, and Zn-COP exhibit evident change from dark orange to light yellow (Figure S14, Supporting Information). Meanwhile, the colors of $Li_2S_6$ solutions with M-COP (M = Mn, Ni, and Zn) are also obviously lighter when compared to that of PVDF and pure $Li_2S_6$. Furthermore, the adsorption property of different binders was proved by the UV–vis absorption spectrum (Figure S15, Supporting Information). The results show that the characteristic peak in the range of 250–300 nm is ascribed to the $S_6^{2-}$ species[40,41] and the absorbance for LiPSs solution was remarkably decreased after adding the M-COP (M = Mn, Ni, and Zn) binders, which further confirms that they can effectively trap the soluble LiPSs and greatly alleviate the shuttle effect in Li–S battery.[42] Moreover, their excellent chemisorption ability has been revealed by the XPS tests (Figure S16, Supporting Information). For instance, two additional peaks (i.e., 167.8 and 169.3 eV) were detected at S 2p spectra for Mn-COP, corresponding to the formation of thiosulfate (166.1–168 eV) and polythionate (168–172 eV) complexes. Due to the increase in sulfur utilization and reduction, the respective peaks of the terminal ($S_T^{-1}$) and bridging ($S_B^0$) sulfur decreased significantly.[43] Besides, the slight shift of peak positions in S 2p spectra to lower binding energy may be attributed the interaction between the thiourea group and the electropositive Li atoms (Figure S16, Supporting Information). In addition, the excellent chemisorption effects were further verified by the cyclic voltammetry (CV) tests of symmetrical cells with the electrolyte containing $Li_2S_6$ only at a scanning rate of 10 mV $S^{-1}$ (Figure S17, Supporting Information), in which the intensity of redox peak and current area in CV curves can evaluate the catalytic intensity of LiPSs.[44] As expected, the symmetrical cell employing Mn-COP binder exhibits higher current area, lower potentials of oxidation and reduction peaks and higher redox peak intensity when compared with PVDF/CNT/S electrode, indicating the easier redox reaction of LiPSs (Figure S17, Supporting Information).

### 2.2. The Electrochemical Performances

After assembling CNT, S, and samples into the electrode, the S content in the electrode was determined to be ≈49 wt% (Figure S18, Supporting Information). Apart from that, in order to further verify the steady electrochemical cyclability of M-COP (M = Mn, Ni, and Zn), the electrochemical performances at different specific current densities were tested in coin-cell configuration. CV curves of cells based on Mn-COP/CNT/S and other reference electrodes were tested in the voltage range of 1.6–2.8 V with a scanning rate of 0.1 mV $s^{-1}$ (**Figure 4**a; Figure S19, Supporting Information). From the good overlap of peak position and peak intensity after the second cycle, it is demonstrated that Mn-COP/CNT/S has a stable redox reaction in the process of the battery cycle. In the first five cycles, two typical cathode peaks and one anode peak can be observed. During the cathode scanning, the anode peak at 2.46 V is generated by the

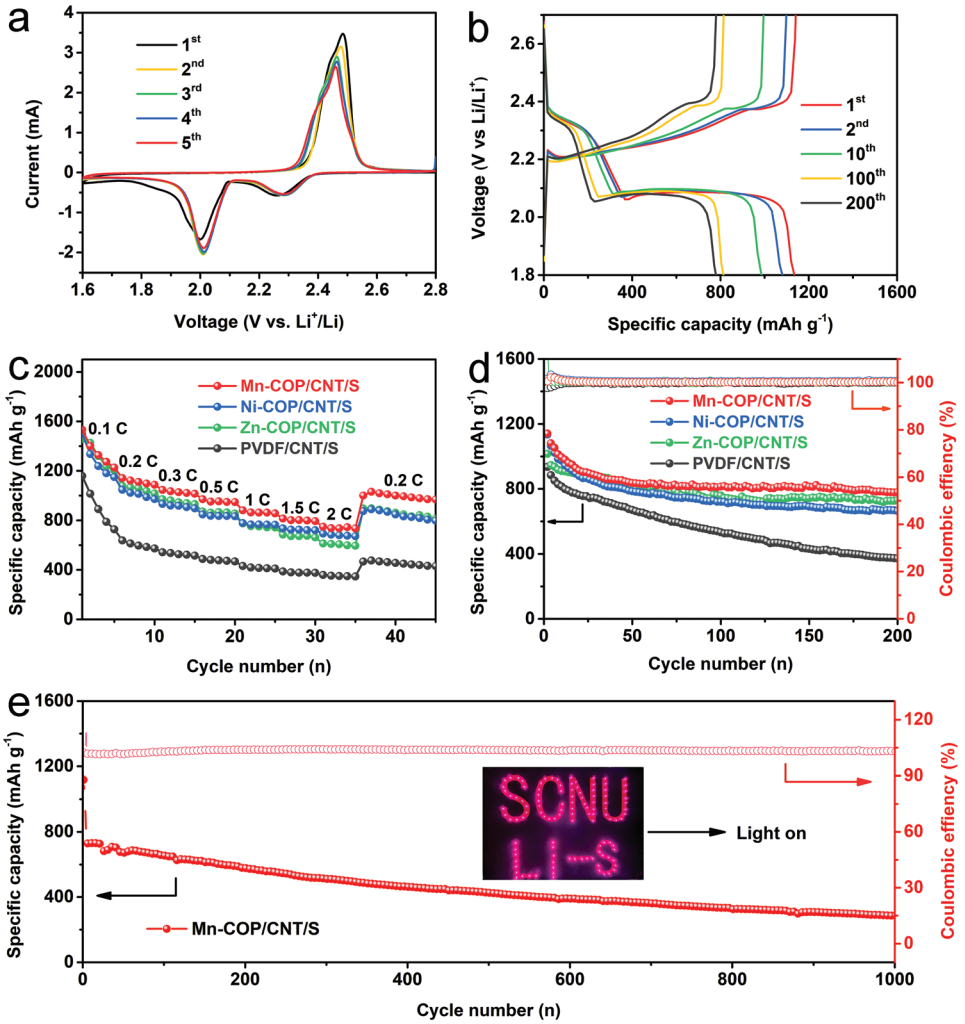


**Figure 4.** Electrochemical performances of Li–S cells with different binders. a) CV curves of Mn-COP/CNT/S based Li–S cell at a scanning rate of 0.1 mV $s^{-1}$ in the voltage range of 1.6–2.8 V. b) Charge–discharge curves of Mn-COP/CNT/S based Li–S cell under different cycle numbers at 0.5 C. c) Rate performance of Li–S cells with different binders. d) Cycling performances of Li–S cells with different binders at 0.5 C. e) Cycling performance of Li–S cell with Mn-COP at 4 C (the inset is the photograph of LED panel lit up).

oxidation of $Li_2S/Li_2S_2$ to $S_8$.[45,46] Additionally, the first reduction peak at ≈2.30 V represents the transition of $S_8$ to long-chain LiPSs ($Li_2S_x$, $4 \le x \le 8$), while the second reduction peak at ≈2.01 V can be attributed to the step-wise conversion of long-chain $Li_2S_x$ to $Li_2S_x$ ($x < 4$) and insoluble $Li_2S_2/Li_2S$, respectively (Figure 4a).[47] Compared with Ni-COP/CNT/S, Zn-COP/CNT/S, and PVDF/CNT/S based cells (Figure S19, Supporting Information), Mn-COP/CNT/S based cell represents obviously lower polarization, which indicates that it has faster redox kinetics and outstanding electrochemical reversibility. Corresponding to the CV results, the constant current charge-discharge curves of the cells based on these binders consist of two clear discharging platforms and one charging platform (Figure 4b; Figure S20, Supporting Information). In addition, Mn-COP/CNT/S based cell has the smallest overpotential for the conversion from long-chain LiPSs to insoluble $Li_2S_2/Li_2S$ (Figure S21, Supporting Information).[48]

In addition, the rate performances of cells with various binders have been systematically evaluated at different rates. By increasing the charge–discharge current density every five cycles, the Mn-COP/CNT/S based cell delivers a highly reversible discharge capacity of 1533.0, 1142.0, 1045.1, 971.3, 881.3, 814.2, and 748.6 mAh $g^{-1}$ at 0.1 C, 0.2 C, 0.3 C, 0.5 C, 1 C, and 2 C, respectively (Figure 4c). When the current density is switched back to 0.2 C, the reversible capacity can still be restored to 1030 mAh $g^{-1}$. In addition, the capacities of Ni-COP/CNT/S and Zn-COP/CNT/S based cells under different current densities are inferior to Mn-COP/CNT/S based cell (Figure 4c). In sharp contrast, the capacities of PVDF/CNT/S based cell decrease sharply under different current densities, suggesting poorer performance than M-COP (M = Mn, Ni, and Zn) based cells. Based on the superior rate performance, we further set to explore other battery properties. After activation, the initial discharge-specific capacity of Mn-COP/CNT/S based cell is as high as 1140 mAh $g^{-1}$ at 0.5 C, and the Coulombic efficiency is nearly 100% (Figure 4d). In contrast, the initial discharge-specific capacities of the cells based on Ni-COP/CNT/S (1134.5 mAh $g^{-1}$) and Zn-COP/CNT/S (1015.3 mAh $g^{-1}$) are

slightly lower than that of Mn-COP/CNT/S based cell. Notably, the initial discharge-specific capacity of PVDF/CNT/S based cell (934.8 mAh $g^{-1}$) is much lower than that of Mn-COP/CNT/S. After 200 cycles, the specific capacity of Mn-COP/CNT/S based cell can be stabilized at 779.9 mAh $g^{-1}$, which is almost twice higher than that of PVDF/CNT/S based cell (371.4 mAh $g^{-1}$) (Figure 4d). The $Li^+$ transference number has been tested and the result shows that Mn-COP is more favorable for $Li^+$ hopping/transferring than PVDF (Figure S22, Supporting Information).

In addition, the porosity and density of Mn-COP/CNT/S are calculated to be 66.41% and 1.71 g $mL^{-1}$, respectively (Figure S23, Supporting Information). The moderate porosity and high density of the electrode would set basis for the superior performance during the battery tests. Moreover, SEM tests were further presented to study the surface morphology of the fresh and cycled electrodes based on different binders (Figures S24 and S25, Supporting Information). It can be clearly observed that the surface morphology of PVDF/CNT/S is severely fractured while the electrode integrity of Mn-COP/CNT/S is well preserved after cycle tests. This might be attributed to the strong adhesion and mechanical strength of Mn-COP that enable to tolerate the volume expansion/contraction during the charge–discharge processes, whereas PVDF chains gradually become scattered and unable to bind the electrode together.[50] Besides, the obvious cracks on the surface of PVDF/CNT/S electrode suggest that it would be hard for the cathode with PVDF binder to operate under higher sulfur loading conditions. SEM cross-section images show that the volume expansion of Mn-COP/CNT/S electrode after cycling is obviously buffered compared with PVDF/CNT/S electrode (Figure S26, Supporting Information). The prolonged cycling tests of Mn-COP/CNT/S and PVDF/CNT/S based cells under high current density have also been demonstrated. Mn-COP/CNT/S based cell exhibits superior initial discharge specific capacity of 1027.6 mAh $g^{-1}$ at 1 C and the Coulombic efficiency is 99.13% (Figure S27, Supporting Information). Even after 600 cycles, its capacity can still be maintained at 442.2 mAh $g^{-1}$ with a 0.095% capacity decay per cycle. In contrast, PVDF/CNT/S based cell suffers from the fast decline of capacity to 170.7 mAh $g^{-1}$ after 600 cycles. Additionally, the initial discharge-specific capacities of Ni-COP and Zn-COP are 948.0 and 879.8 mAh $g^{-1}$ with the capacity decay of 0.120% and 0.114% per cycle, respectively, which are still poorer than that of Mn-COP/CNT/S based cell. Even at 2 C, the Mn-COP/CNT/S based cell exhibits excellent cycling stability with 0.068% decay per cycle, which is superior to that of PVDF/CNT/S based cell (Figure S28, Supporting Information). Notably, excellent cycling stability for >1000 cycles (0.064% decay per cycle) is achieved at 4 C (Figure 4e). Interestingly, the Mn-COP/CNT/S based Li–S cell can be used to light up a light-emitting diode (LED) panel for further verification experiments (inset in Figure 4e). Even when S loading is as high as 70%, the Mn-COP/CNT/S based cell presents good initial specific capacity of 815.6 mAh $g^{-1}$ at 0.5 C and it can be stabilized for 100 cycles (Figure S29, Supporting Information). We further perform the entire galvanostatic intermittent titration technique (GITT) discharge process tests and the results show that M-COP (M = Mn, Ni, and Zn) can utilize more sulfur than that of PVDF (Figure S30, Supporting Information). Specifically, the sulfur utilization of the cell with Mn-COP is as high as 81.8%, which is much higher than that of the cells with Ni-COP (70.3%) and Zn-COP (74.1%) (Figure S30, Supporting Information). The excellent prolonged cycling performance suggests that the superiority of Mn-COP to contrast samples in stabilizing the electrode. Furthermore, the electrochemical impedance spectroscopy (EIS) Nyquist plots consisting of a depressed semicircle are observed for all of the electrodes (Figure S31, Supporting Information), in which the diameter of the depressed semicircle $R_{ct}$ ($R_{ct}$, semicircle diameter) corresponds to the charge-transfer resistance.[17] Before cycling, the Mn-COP/CNT/S based cell has a lower $R_{ct}$ value than those of the Ni-COP/CNT/S, Zn-COP/CNT/S, and PVDF/CNT/S based cells, suggesting that the Mn-COP binder is more beneficial to reduce the $R_{ct}$. After 200 cycles, all of the semicircles are reduced, which might be due to the activation of the electrode during the charge-discharge processes. Besides, a concave second semicircle appears in the EIS curves (Figure S32, Supporting Information). The semicircle in the high frequency region (left) is due to the surface contact resistance ($R_{int}$) between the electrolyte and the cathode.[49] As compared with the other three electrodes, the Mn-COP/CNT/S based cell still maintains the lowest $R_{ct}$ and $R_{int}$, and the charge transfer resistances of Mn-COP/CNT/S, Ni-COP/CNT/S, Zn-COP/CNT/S, and PVDF/CNT/S based cells increase in turn, indicating the superiority of Mn-COP binder in keeping the integrity and continuous conductive path of the electrode.

Nowadays, the conditions with lean electrolyte and high sulfur loading are gradually regarded as vital evaluation indexes of the practical application potential of Li–S battery.[51] Based on this, we also assembled a Mn-COP/CNT/S electrode with a relatively low E/S ratio of 8.1 µL $mg^{-1}$ and a sulfur loading of 4.0 mg $cm^{-2}$, and the cell delivers a high specific capacity of 1029.9 mAh $g^{-1}$, which further stabilizes at 610.0 mAh $g^{-1}$ after 100 cycles (Figure S33, Supporting Information). Even when the E/S ratio is reduced to 5.8 µL $mg^{-1}$ coupling with a higher sulfur loading (5.5 mg $cm^{-2}$), the cell can still exhibit an excellent capacity of 949.2 mAh $g^{-1}$ (Figure S34, Supporting Information). Based on the above results, we further set out to explore the performances of batteries with higher sulfur loading. Noteworthy, Mn-COP/CNT/S based cell enables the high sulfur loading of 8.6 mg $cm^{-2}$ (sulfur loading of "4H", >8.0 mg $cm^{-2}$), in which the achieved initial area capacity and specific capacity are 7.8 mA h $cm^{-2}$ and 909.8 mA h $g^{-1}$ at 0.1 C, respectively (Figure S35, Supporting Information). Generally, the Mn-COP binder helps to maintain the excellent capacity and cycling stability of the cell under conditions of high sulfur loading and lean electrolyte, indicating that our work is competitive and ahead of the currently reported work status (Tables S1,S2, Supporting Information).

To further evaluate the electrochemical stability, CV curves of Mn-COP/CNT/PVDF based cell have been studied. There is no redox peak in the voltage window of 1.6–2.8 V, indicating the good electrochemical stability of Mn-COP that it will not affect the redox reaction of sulfide in the cell (Figure S36, Supporting Information). In addition, different contents (i.e., 5–20 wt%) of binders have also been studied to explore the optimal specific gravity of binder in the cathode as the conductivity and mechanical strength of the cathodes are both

important parameters for Li–S batteries. After tests, M-COP (M = Mn, Ni, and Zn) based cells all show the best battery performances with the optimized binder content of 10 wt% (Figures S37 and S38, Supporting Information). Moreover, we further set out to compare the performances of them with traditional polymer binders (e.g., sodium carboxymethylcellulose (CMC), sodium alginate (SA) and LA132, etc.) (Figure S39, Supporting Information). However, the cells with these traditional polymer binders all show obvious capacity decay after 200 cycles at 0.5 C, which further proves the superiority of Mn-COP in stabilizing the electrochemical properties. In addition, TAPP-COP without coordination metal has also been evaluated as the binder. Although the performance is much lower than that of Mn-COP based cell, it is still slightly higher than that of PVDF based cell, suggesting the vital role of Mn-porphyrin in enhancing the battery properties (Figure S40, Supporting Information).

Moreover, density functional theory (DFT) calculations were conducted to further reveal the vital roles of M-COP (M = Mn, Ni, and Zn) in battery processes. We import DFT calculation to gain an atomic understanding of the charge-discharge process in the sulfur electrode, with the details given in supporting information. By measuring the collective bonding length of $Li_2S$ on M-TAPP (M = Mn, Ni, and Zn) and PVDF (**Figure 5**a; Figure S41, Supporting Information), we find the bond length between Li and the adsorption site is lower on Mn-TAPP than

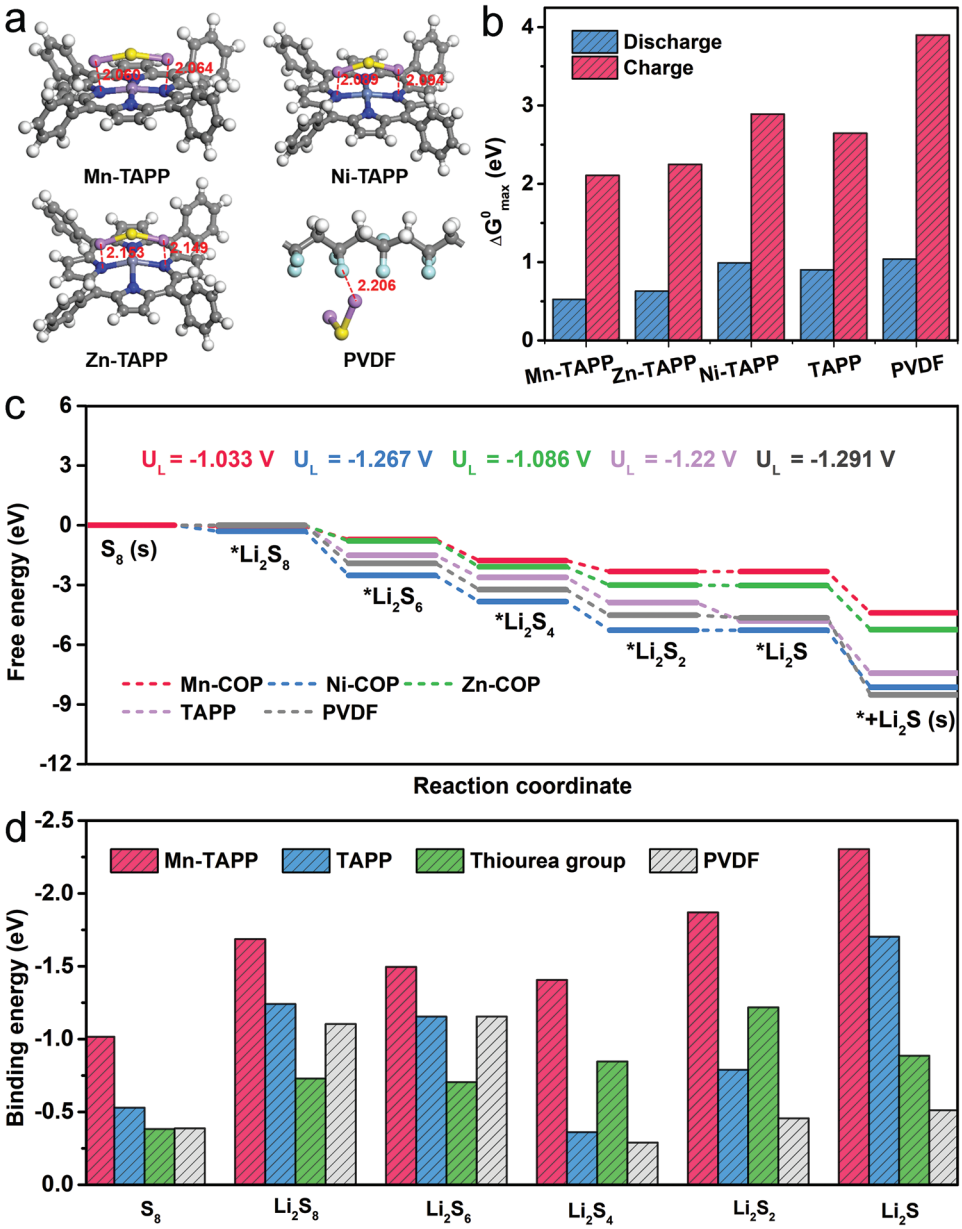


**Figure 5.** DFT calculations of different binders. a) The virtualized position of the bond lengths of N/F–Li between the adsorbed $Li_2S$ clip and the substrate. b) The $\Delta G^0_{max}$ values for the charge and discharge processes on each site. c) The reaction free energy diagrams of the discharge process in the sulfur electrode. d) The binding energy of $Li_2S_x$ on Mn-TAPP, TAPP, thiourea group, and PVDF.

in the other three structures. These indicate the higher affinity of Mn-TAPP to the adsorbates. Moreover, the associated largest Gibbs energy among the elementary steps ($\Delta G^0_{max}$) and the free energy diagrams (FED) of the reaction process on M-COP (M = Mn, Ni, and Zn) and PVDF are plotted (Figure 5b; Figure S42, Supporting Information). The $\Delta G^0_{max}$ value can be connected with the activity by $k \exp(-ß\Delta G^0_{max}/RT)$, with $K$ and $ß$ as the kinetic constant and symmetrical factor. We find these values of $\Delta G^0_{max}$, though seemingly large, can be conquered by a small overpotential. The relative free energy profiles show the associated "limiting potential" (an indicator of the request overpotential to start the electrocatalytic reaction) for the discharge process (Figure 5c), where we find the overpotential is within 0.55 V for all the materials, indicating they all have the activities. Besides, we find the Mn-COP possesses the smallest $\Delta G^0_{max}$ for the charge and discharge processes, respectively, indicating it is the best catalyst for both the discharge and charge process. The good activity for both charging and discharging processes can be attributed to the higher reactivity of Mn-COP, which accords with the collective optimized structures of LiPSs adsorption on the associated groups and the adsorption energy collected (Figure 5d; Figures S43–S45, Supporting Information). As expected, the adsorption energy is generally larger on Mn-COP than on other structures. The energy diagram indicates the adsorption of the intermediates is generally weaker than the optimal value, increasing its affinity will hence result in a better activity (Figure S46, Supporting Information). Above all, Mn-COP exhibits the best LiPSs adsorption/catalysis ability in the DFT calculations, which is well consistent with above-mentioned experimental results.

## 3. Conclusion

In summary, an in situ cathode interweaving strategy has been proposed based on a series metalloporphyrin based M-COP (M = Mn, Ni, and Zn) binders, during which the in situ heating polymerization of binders can simultaneously provide strong interaction with cathodic materials and accomplish one-pot cathode fabrication. Thus obtained M-COP (M = Mn, Ni, and Zn) exhibit excellent mechanical strengths, polysulfides adsorption/catalysis and $Li^+$ hopping/transferring ability. Specifically, the modulus of Mn-COP can reach up to ≈54.60 GPa (≈40 times higher than PVDF), which can tightly interweave cathodic materials (i.e., CNT and S) as a compact whole and be facilely fabricated in large scale (≈20 cm in a batch experiment). Best of them, Mn-COP/CNT/S based cell delivers an initial specific capacity of 1027 mAh $g^{-1}$ at 1 C, 913 mAh $g^{-1}$ at 2 C, and an excellent cycling stability for >1000 cycles (0.064% decay per cycle) at 4 C. Moreover, the cell exhibits a high specific capacity of 1029.9 mAh $g^{-1}$ at a low E/S ratio of 8.1 µL $mg^{-1}$, and excellent capacity of 949.2 mAh $g^{-1}$ even when the E/S ratio is reduced to 5.8 µL $mg^{-1}$, which suppress almost all of the other traditional binders. Noteworthy, Mn-COP based cell delivers excellent capacities at a high sulfur-loading (8.6 mg $cm^{-2}$) and low E/S ratio (5.8 µL $mg^{-1}$), and the utilization-rate of sulfur is as high as 81.8%, which is the optimal binder performance in Li–S battery as far as we know and has much potential to meet the "4H" and "4L" criteria. Furthermore, its excellent electrochemical performance was confirmed by DFT calculations and other characterizations, which reveals the important functions of metalloporphyrin and thiourea groups in LiPSs adsorption/catalysis and $Li^+$ hopping/transferring. This work provides a new guidance of cathode fabrication techniques based on a series of powerful metalloporphyrin based binders, which would facilitate the exploration of novel binder chemistry to meet the high requirements of next-generation Li–S battery.

## 4. Experimental Section

*Synthesis of M-TAPP (M = Mn, Ni, and Zn)*: The syntheses of M-TAPP (M = Mn, Ni, and Zn) followed previously reported method.[52] TAPP (200 mg, 0.3 mmol) and relative metal acetate salt (0.75 mmol) were added in a mixed solution of methanol (20 mL), chloroform (90 mL), and DMF (30 mL). The flask was first treated with $N_2$ purification for three times and heated under stirring at 80 °C under $N_2$ for 24 h. After cooling to the room temperature, the solution was filtered and washed with a large amount of water. Then, the product was dried at 60 °C under vacuum.

*Synthesis of M-COP (M = Mn, Ni, and Zn)*: M-TAPP (M = Mn, Ni, and Zn) (0.03 mmol) and PDI (0.06 mmol) were dissolved in NMP (500 mL) separately. After standing in the air for 30 min, a kind dark gel was obtained. If the resultant solution was casted on a substrate with a doctor blade and thoroughly dried at 60 °C for 12 h, the M-COP based flexible films could be obtained and easily peeled off from the substrate.

*Fabrication of Cathodes*: Sulfur cathodes were fabricated by a slurry casting method. The sulfur (70 wt%) and CNT (30 wt%) were mixed and heated at 155 °C in a sealed tube for 12 h to prepare the carbon-sulfur composite. As for the cathodes, 70 wt% CNT/S composite, 20 wt% CNT, and 10 wt% M-COP precursor (molar ratio, TAPP : PDI = 1 : 2) were mixed in NMP to form a slurry, then casted on aluminum current collectors and heated at 60 °C for 12 h. The sulfur content in this work was determined to be 49 wt%. To investigate the generality for M-COP, the properties of various binders (i.e., PVDF, sodium alginate (SA), sodium carboxymethylcellulose (CMC), and LA132) were applied through the similar preparation processes for Li–S cell tests.

*Preparation of Electrolyte $Li_2S_6$*: The electrolyte $Li_2S_6$ was prepared by adding $Li_2S$ and sulfur powder at a certain molar ratio of 1 : 3 into DME and DOL mixed solution (v/v, 1 : 1). Then, 1.0 M lithium bis(trifluoromethane sulfonyl)imide (LiTFSI) salt was added and stirred for 24 h. The static adsorption of polysulfides was carried out using the concentration of 0.03 M $Li_2S_6$ electrolyte.

## Supporting Information

Supporting Information is available from the Wiley Online Library or from the author.

## Acknowledgements

This work was financially supported by the NSFC (Grants 22171139, 21871141, 21871142, 21901122, 22071109, and 22225109), the Postdoctoral Innovation Talent Support Program (BX20220115), and Guangzhou Basic and China Postdoctoral Science Foundation (No. 2021M701270).

## Conflict of Interest

The authors declare no conflict of interest.

## Author Contributions

X.-M.Y. and C.G. contributed equally to this work. Y.-Q.L., Y.C., and X.Y. conceived the idea. X.Y. designed the experiments, collected and

 

analyzed the data. C.G., C.S., M.L., Y.Z., J.Z., and H.D. assisted with the experiments and characterizations. X.Y. wrote the manuscript. All authors have approved the final version of the manuscript.

## Data Availability Statement

The data that support the findings of this study are available from the corresponding author upon reasonable request.

## Keywords

in situ interweaving strategy, Li–S cathode, lithium polysulfides, metalloporphyrin, polymer binder

Received: September 26, 2022
Revised: November 10, 2022
Published online:

[1] Y. Huang, L. Lin, C. Zhang, L. Liu, Y. Li, Z. Qiao, J. Lin, Q. Wei, L. Wang, Q. Xie, D.-L. Peng, *Adv. Sci.* **2022**, *9*, 2106004.
[2] Z. W. Seh, Y. Sun, Q. Zhang, Y. Cui, *Chem. Soc. Rev.* **2016**, *45*, 5605.
[3] H. Yuan, J.-Q. Huang, H.-J. Peng, M.-M. Titirici, R. Xiang, R. Chen, Q. Liu, Q. Zhang, *Adv. Energy Mater.* **2018**, *8*, 1802107.
[4] C.-L. Song, Z.-H. Li, L.-Y. Ma, M.-Z. Li, S. Huang, X.-J. Hong, Y.-P. Cai, Y.-Q. Lan, *ACS Nano* **2021**, *15*, 13436.
[5] G. Zhou, H. Chen, Y. Cui, *Nat. Energy* **2022**, *7*, 312.
[6] F. Zou, A. Manthiram, *Adv. Energy Mater.* **2020**, *10*, 2002508.
[7] P. T. Dirlam, R. S. Glass, K. Char, J. Pyun, *J. Polym. Sci. Polym. Chem.* **2017**, *55*, 1635.
[8] K. Yang, L. Yang, Z. Wang, B. Guo, Z. Song, Y. Fu, Y. Ji, M. Liu, W. Zhao, X. Liu, S. Yang, F. Pan, *Adv. Energy Mater.* **2021**, *11*, 2100601.
[9] Q. Zhang, Q. Huang, S.-M. Hao, S. Deng, Q. He, Z. Lin, Y. Yang, *Adv. Sci.* **2022**, *9*, 2103798.
[10] C. Senthil, S.-S. Kim, H. Y. Jung, *Nat. Commun.* **2022**, *13*, 145.
[11] R. Sun, J. Hu, X. Shi, J. Wang, X. Zheng, Y. Zhang, B. Han, K. Xia, Q. Gao, C. Zhou, L. Mai, *Adv. Funct. Mater.* **2021**, *31*, 2104858.
[12] H. Wang, V. Sencadas, G. Gao, H. Gao, A. Du, H. Liu, Z. Guo, *Nano Energy* **2016**, *26*, 722.
[13] Q. Pang, X. Liang, C. Y. Kwok, J. Kulisch, L. F. Nazar, *Adv. Energy Mater.* **2017**, *7*, 1601630.
[14] P. Bhattacharya, M. I. Nandasiri, D. Lv, A. M. Schwarz, J. T. Darsell, W. A. Henderson, D. A. Tomalia, J. Liu, J.-G. Zhang, J. Xiao, *Nano Energy* **2016**, *19*, 176.
[15] W. Chen, T. Qian, J. Xiong, N. Xu, X. Liu, J. Liu, J. Zhou, X. Shen, T. Yang, Y. Chen, C. Yan, *Adv. Mater.* **2017**, *29*, 1605160.
[16] C. Guo, M. Liu, G.-K. Gao, X. Tian, J. Zhou, L.-Z. Dong, Q. Li, Y. Chen, S.-L. Li, Y.-Q. Lan, *Angew. Chem., Int. Ed.* **2022**, *61*, e202113315.
[17] G. Yoo, S. Kim, C. Chanthad, M. Cho, Y. Lee, *Chem. Eng. J.* **2021**, *405*, 126628.
[18] M. Müller, L. Pfaffmann, S. Jaiser, M. Baunach, V. Trouillet, F. Scheiba, P. Scharfer, W. Schabel, W. Bauer, *J. Power Sources* **2017**, *340*, 1.
[19] Y. Wang, G. Cao, *Adv. Mater.* **2008**, *20*, 2251.
[20] L. Ji, Z. Lin, M. Alcoutlabi, X. Zhang, *Environ. Sci.* **2011**, *4*, 2682.
[21] X. Gao, Q. Sun, X. Yang, J. Liang, A. Koo, W. Li, J. Liang, J. Wang, R. Li, F. B. Holness, A. D. Price, S. Yang, T.-K. Sham, X. Sun, *Nano Energy* **2019**, *56*, 595.
[22] M. R. Kaiser, X. Liang, H.-K. Liu, S.-X. Dou, J.-Z. Wang, *Carbon* **2016**, *103*, 163.
[23] Y. Zhang, X. Zhang, S. R. P. Silva, B. Ding, P. Zhang, G. Shao, *Adv. Sci.* **2022**, *9*, 2103879.
[24] E. Azaceta, S. García, O. Leonet, M. Beltrán, I. Gómez, A. Chuvilin, A. R. Mainar, J. A. Blazquez, M. Knez, *Mater. Today Energy* **2020**, *18*, 100567.
[25] Y. Yang, G. Zheng, S. Misra, J. Nelson, M. F. Toney, Y. Cui, *J. Am. Chem. Soc.* **2012**, *134*, 15387.
[26] Y.-L. Yang, Y.-R. Wang, G.-K. Gao, M. Liu, C. Miao, L.-Y. Li, W. Cheng, Z.-Y. Zhao, Y. Chen, Z. Xin, S.-L. Li, D.-S. Li, Y.-Q. Lan, *Chin. Chem. Lett.* **2022**, *33*, 1439.
[27] N. Keller, M. Calik, D. Sharapa, H. R. Soni, P. M. Zehetmaier, S. Rager, F. Auras, A. C. Jakowetz, A. Görling, T. Clark, T. Bein, *J. Am. Chem. Soc.* **2018**, *140*, 16544.
[28] B. P. Biswal, S. Valligatla, M. Wang, T. Banerjee, N. A. Saad, B. M. K. Mariserla, N. Chandrasekhar, D. Becker, M. Addicoat, I. Senkovska, R. Berger, D. N. Rao, S. Kaskel, X. Feng, *Angew. Chem., Int. Ed.* **2019**, *58*, 6896.
[29] X. Hu, J. Jian, Z. Fang, L. Zhong, Z. Yuan, M. Yang, S. Ren, Q. Zhang, X. Chen, D. Yu, *Energy Storage Mater.* **2019**, *22*, 40.
[30] R.-X. Yang, Y.-R. Wang, G.-K. Gao, L. Chen, Y. Chen, S.-L. Li, Y.-Q. Lan, *Small Struct.* **2021**, *2*, 2100012.
[31] P. L. Cheung, S. K. Lee, C. P. Kubiak, *Chem. Mater.* **2019**, *31*, 1908.
[32] Y. Lu, J.-L. Qin, T. Shen, Y.-F. Yu, K. Chen, Y.-Z. Hu, J.-N. Liang, M.-X. Gong, J.-J. Zhang, D.-L. Wang, *Adv. Energy Mater.* **2021**, *11*, 2101780.
[33] D. W. Kim, C. Senthil, S. M. Jung, S.-S. Kim, H.-S. Kim, J. W. Hong, J.-H. Ahn, H. Y. Jung, *Energy Storage Mater.* **2022**, *47*, 472.
[34] J.-Y. Yue, Y.-T. Wang, X. Wu, P. Yang, Y. Ma, X.-H. Liu, B. Tang, *Chem. Commun.* **2021**, *57*, 12619.
[35] Y. Huang, M. Shaibani, T. D. Gamot, M. Wang, P. Jovanović, M. C. Dilusha Cooray, M. S. Mirshekarloo, R. J. Mulder, N. V. Medhekar, M. R. Hill, M. Majumder, *Nat. Commun.* **2021**, *12*, 5375.
[36] Y. Yang, J. Qiu, L. Cai, C. Liu, S. Wu, X. Wei, D. Luo, B. Zhang, X. Yang, K. N. Hui, J. Liu, Z. Lin, *ACS Appl. Mater. Interfaces* **2021**, *13*, 33066.
[37] J. Qiu, S. Wu, Y. Yang, H. Xiao, X. Wei, B. Zhang, K. N. Hui, Z. Lin, *ACS Appl. Mater. Interfaces* **2021**, *13*, 55092.
[38] H. Wang, M. Ling, Y. Bai, S. Chen, Y. Yuan, G. Liu, C. Wu, F. Wu, *J. Mater. Chem.* **2018**, *6*, 6959.
[39] S. Kim, M. Cho, Y. Lee, *Adv. Funct. Mater.* **2020**, *30*, 1907680.
[40] J. Liu, H. Li, J. Wang, Y. Zhang, D. Luo, Y. Zhao, Y. Li, A. Yu, X. Wang, Z. Chen, *Adv. Energy Mater.* **2021**, *11*, 2101926.
[41] G. Zhou, K. Liu, Y. Fan, M. Yuan, B. Liu, W. Liu, F. Shi, Y. Liu, W. Chen, J. Lopez, D. Zhuo, J. Zhao, Y. Tsao, X. Huang, Q. Zhang, Y. Cui, *ACS Cent. Sci.* **2018**, *4*, 260.
[42] G. Zhou, Y. Zhao, C. Zu, A. Manthiram, *Nano Energy* **2015**, *12*, 240.
[43] B. Jin, D. Wang, J. Zhu, H. Guo, Y. Hou, X. Gao, J. Lu, X. Zhan, X. He, Q. Zhang, *Adv. Funct. Mater.* **2021**, *31*, 2104433.
[44] C. Wang, R. Liu, Y. Fang, W. Yang, F. Jin, M. Gu, D. Zhang, L. He, W. Liu, J. Chen, X. Lin, X. Feng, Y. Ma, *ACS Appl. Nano Mater.* **2022**, *5*, 3531.
[45] X. Fan, R. Yuan, J. Lei, X. Lin, P. Xu, X. Cui, L. Cao, M. Zheng, Q. Dong, *ACS Nano* **2020**, *14*, 15884.
[46] M. Li, J. Zhang, Y. Gao, X. Wang, Y. Zhang, S. Zhang, *J. Mater. Chem.* **2021**, *9*, 2375.
[47] G. Wen, S. Rehman, T. G. Tranter, D. Ghosh, Z. Chen, J. T. Gostick, M. A. Pope, *Chem. Mater.* **2020**, *32*, 4518.
[48] D. Sun, J. Zhou, D. Rao, L. Zhu, S. Niu, J. Cai, Y. Fang, Y. Liu, X. Liu, Y. Zang, Y. Wu, Y. Xie, Z. Zhu, D. Niu, Z. Lu, Z. Pei, G. Wang, *Sustainable Mater. Technol.* **2021**, *28*, e00271.
[49] S. Chen, Z. Song, Y. Ji, K. Yang, J. Fang, L. Wang, Z. Wang, Y. Zhao, Y. Zhao, L. Yang, F. Pan, *Small Methods* **2021**, *5*, 2100839.
[50] J. Oh, S. H. Choi, B. Chang, J. Lee, T. Lee, N. Lee, H. Kim, Y. Kim, G. Im, S. Lee, J. W. Choi, *ACS Energy Lett.* **2022**, *7*, 1374.
[51] S. Li, W. Xiao, H. Do, H. Yang, X. Xu, C. Peng, *Small* **2022**, *18*, 2107109.
[52] S. Lin, S. D. Christian, Y.-B. Zhang, N. Kornienko, M. N. Eva, Y. Zhao, R. P. Aubrey, D. Kim, P. Yang, M. Y. Omar, J. C. Christopher, *Science* **2015**, *349*, 1208.